



ChemComm

**Red to Near-Infrared Phosphorescent Ir(III) Complexes
with Electron-Rich Chelating Ligands**

Journal:	<i>ChemComm</i>
Manuscript ID	CC-FEA-12-2020-008067.R1
Article Type:	Feature Article

SCHOLARONE™
Manuscripts

ARTICLE

Red to Near-Infrared Phosphorescent Ir(III) Complexes with Electron-Rich Chelating Ligands

Sungwon Yoon and Thomas S. Teets*

Received 00th January 20xx,
Accepted 00th January 20xx

DOI: 10.1039/x0xx00000x

The design of molecular phosphors with near-unity photoluminescence quantum yields in the low-energy regions of the spectrum, red to near-infrared, is a long-standing challenge. Because of the energy gap law and the quantum mechanical dependence of radiative decay rate on the excited-state energy, compounds which luminesce in this region of the spectrum typically suffer from low quantum yields. In this article, we highlight our group's advances in the design of top-performing cyclometalated iridium complexes which phosphoresce in red to near-infrared regions. The compounds we have introduced in this body of work have the general formula $\text{Ir}(\text{C}^{\wedge}\text{N})_2(\text{L}^{\wedge}\text{X})$, where $\text{C}^{\wedge}\text{N}$ is a cyclometalating ligand that controls the photoluminescence color and $\text{L}^{\wedge}\text{X}$ is a monoanionic chelating ancillary ligand. The $\text{Ir}(\text{C}^{\wedge}\text{N})_2(\text{L}^{\wedge}\text{X})$ structure type is among the most widely studied and technologically successful classes of molecular phosphors, particularly when $\text{L}^{\wedge}\text{X}$ = acetylacetonate (acac). In our work we have pioneered the use of electron-rich, nitrogen containing ancillary ($\text{L}^{\wedge}\text{X}$) ligands as a means of controlling the excited-state dynamics and optimizing them to give record-breaking phosphorescence quantum yields. This paper progresses through our work in three distinct regions of the spectrum – red, deep-red, and near-infrared – and summarizes the many insights we have gained on the relationships between molecular structure, frontier orbital energies, and excited-state dynamics.

Introduction

Molecular phosphors and their applications

Phosphorescent coordination compounds, many of them organometallic compounds with one or more metal-carbon bond, have been studied both for their fundamental photophysics¹ and for their many applications.^{2,3} There are numerous fruitful applications of phosphorescent compounds, including luminescent sensing in biological contexts,^{4–7} and many related compounds have been widely used as photosensitizers for organic photoredox catalysis and solar fuels applications.^{8,9} However, arguably the most widely studied context for phosphorescent organometallic compounds, and certainly the most commercially successful, has been in electroluminescent devices for display technologies. Among these, organic light-emitting diodes (OLEDs) have made the biggest mark.^{2,10,11} Compared to fluorescent materials, which typically have maximum theoretical OLED efficiencies of 25%, phosphorescent dopants result in much higher theoretical and practical OLED device efficiencies, on account of their unity exciton harvesting efficiencies. There have been many classes of phosphorescent molecules investigated as OLED dopants, with cyclometalated iridium compounds quickly emerging as the champion OLED emitters since they were first used for this application over 20 years ago,¹² very early in the development

of phosphorescent OLEDs (sometimes abbreviated as PhOLEDs).

Cyclometalated iridium structure classes

Cyclometalated iridium complexes encompass several structure types which can be categorized in different ways, but in the limiting extremes there are two main categories – homoleptic tris-cyclometalated *fac/mer*- $\text{Ir}(\text{C}^{\wedge}\text{N})_3$, and heteroleptic bis-cyclometalated complexes where the $[\text{Ir}(\text{C}^{\wedge}\text{N})_2]^+$ fragment has its two remaining cis-oriented coordination sites occupied by one bidentate or two monodentate ancillary ligands. Fig. 1 summarizes the common cyclometalated iridium structure types. In these compounds Ir is always in the +3 formal oxidation state with pseudo-octahedral coordination, and “ $\text{C}^{\wedge}\text{N}$ ” represents a cyclometalating ligand, which binds the metal through an organometallic Ir–aryl linkage and through a nitrogen-based L-donor moiety. The prototypical cyclometalating ligand is 2-phenylpyridine, which was used in the earliest reports of cyclometalated iridium complexes from Watts and co-workers over thirty years ago.¹³ Among heteroleptic structures, the $[\text{Ir}(\text{C}^{\wedge}\text{N})_2(\text{N}^{\wedge}\text{N})]^+$ class, where $\text{N}^{\wedge}\text{N}$ is a neutral chelating ligand from the 2,2'-bipyridine class, is among the most widely studied and has become particularly prominent in the field of photoredox catalysis.^{8,14,15} However, in the OLED field charge-neutral complexes are preferable since they can be thermally evaporated, and $\text{Ir}(\text{C}^{\wedge}\text{N})_2(\text{L}^{\wedge}\text{X})$ complexes, where $\text{L}^{\wedge}\text{X}$ is a monoanionic chelating ligand, have had a huge impact. In particular, the $\text{Ir}(\text{C}^{\wedge}\text{N})_2(\text{acac})$ (acac = acetylacetonate) family of compounds has become especially prominent in OLED research, since first being introduced by Lamansky et al.^{11,16}

Department of Chemistry, University of Houston, 3585 Cullen Blvd. Room 112, Houston, TX 77204-5003, USA Email: tteets@uh.edu

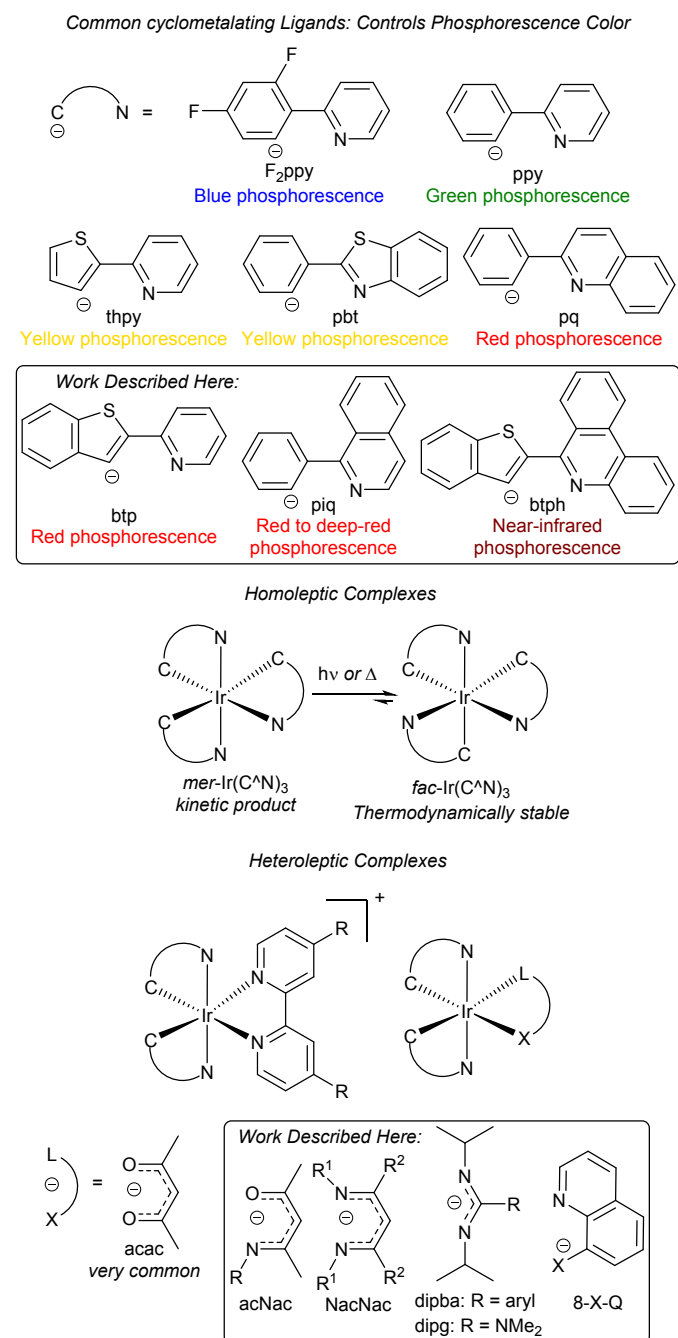


Fig. 1. Common cyclometalated iridium structure types with representative cyclometalating (C^N) and ancillary (L^X) ligands.

The Red/NIR challenge

In most cyclometalated iridium complexes, particularly the common *fac*-Ir(C^N)₃ and Ir(C^N)₂(acac) varieties, the photoluminescence color is controlled by the structure of the cyclometalating (C^N) ligand. As shown in Fig. 1, the color can be tuned throughout the visible range and into the NIR by changing the C^N ligand. Green-phosphorescent cyclometalated iridium complexes, often supported by C^N = 2-phenylpyridine (ppy), have very high photoluminescence quantum yields (Φ_{PL})¹⁷ and have been used in OLED devices¹² which are efficient and stable enough to be commercialized.

The lack of efficient and stable blue-phosphorescent complexes remains the biggest bottleneck in the color display industry and presents its own set of unique design challenges. We^{18–20} and many others^{17,21–23} have introduced new designs of blue-phosphorescent complexes to tackle this challenge, but those advances will not be covered here. The topic of this article is the opposite extreme of the spectrum, the red to near-infrared. While it is true that red OLED devices with cyclometalated iridium complexes have been commercialized and their improvement is not a major focus in industry, the efficiency of red OLEDs is less than that of green, and that is largely because of the inherently lower quantum yields of red-phosphorescent cyclometalated iridium complexes. There are many examples of cyclometalated iridium complexes throughout most of the visible spectrum (blue-green to orange) that have near-unity Φ_{PL} . As shown in Fig. 2 the red-phosphorescent compounds that have been used in the top-performing red OLEDs (maximum emission $\lambda_{\text{em}} \sim 600\text{--}650$ nm), at least from what is available in the academic literature, have Φ_{PL} values that top out at ~ 0.5 .^{11,24,25} Quantum yields in the deep-red region ($\lambda_{\text{em}} \sim 650\text{--}700$ nm) and near-infrared (NIR) region ($\lambda_{\text{em}} > 700$ nm) fall off even more, such that most NIR iridium phosphors have $\Phi_{\text{PL}} < 0.1$.⁶ Strategies to improve Φ_{PL} in these low-energy regions may have an impact on red OLED design for color displays, as well as other applications where red to NIR phosphorescence is important, while also addressing the longstanding fundamental challenge of achieving high photoluminescence quantum yields for red to NIR emission.

To understand why efficient red luminescence is difficult to achieve, it is first necessary to consider the definition of photoluminescence quantum yield (Φ_{PL}) and its kinetic origin:

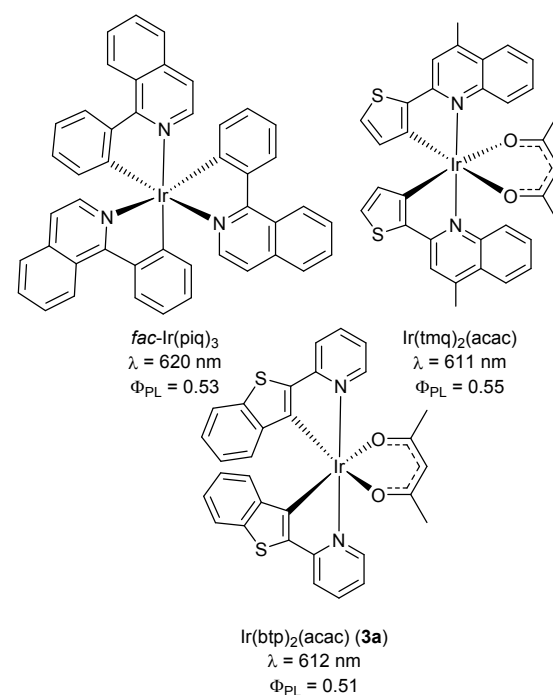


Fig. 2. Structures of cyclometalated iridium complexes used in top-performing red OLED devices.^{11,24,25}

$$\Phi_{\text{PL}} = \frac{\text{emitted photons}}{\text{absorbed photons}} = \frac{k_r}{k_r + k_{\text{nr}}} \quad (1)$$

As given by Equation 1 above, Φ_{PL} is an efficiency ratio that is dictated by two rate constants. The radiative rate constant, k_r , is the first-order rate constant associated with radiative decay from the excited state, i.e. the rate constant at which photons are generated from the excited state. The nonradiative rate constant, k_{nr} , is the sum of the first-order rate constants for all other processes that thermally deactivate the excited state, without generating a photon. From second-order perturbation theory, the radiative rate constant is given by Equation 2 below:²

$$k_r = \text{const} \times \Delta E^{-3} \times \left| \sum_{S_n} \frac{\langle \varphi_{S_n} | \hat{H} | \varphi_{T_1} \rangle}{E_{T_1} - E_{S_n}} \times \underbrace{\langle \varphi_{S_0} | \text{er} | \varphi_{S_n} \rangle}_{\text{transition dipole}} \right|^2 \quad (2)$$

The ΔE term in Equation 2 is the energy gap between the ground and excited states. As a result, compounds with low-energy excited states that emit in the red to near-infrared regions tend to have smaller k_r values than structurally related compounds that emit from higher-energy excited states. In addition, the well-known Energy Gap Law²⁶ stipulates a negative exponential relationship between k_{nr} and ΔE , given by Equation 3 where γ is a molecular-specific term and ω_M is the dominant vibrational frequency in the system.²⁷

$$k_{\text{nr}} \propto \exp(-\gamma \Delta E / \hbar \omega_M) \quad (3)$$

Thus, k_{nr} tends to *increase* when emission occurs from a lower-energy state, as a result of greater vibrational coupling between the ground and excited state. Both the quantum mechanical dependence of k_r (Equation 2) and the Energy Gap Law (Equation 3) contribute to the inherently low photoluminescence quantum yields of red to NIR molecular phosphors.

Electronic Structure and Excited States

In order to maximize Φ_{PL} , one must maximize k_r and minimize k_{nr} . The most common strategy to minimize k_{nr} is to make the molecule more rigid, which restricts the vibrational modes responsible for nonradiative decay. We have used this strategy to some success in our own research, as described later, but at the heart of our approach is the ability to maximize k_r via judicious ancillary ligand choice. To understand how that is possible, it is necessary to consider the frontier orbitals and excited states of typical cyclometalated iridium compounds, how they relate to the radiative rate constant, and how ligand design can influence excited-state landscape. Fig. 3 shows a simplified frontier orbital diagram for a cyclometalated iridium complex, showing both d orbitals on the Ir and π and π^* orbitals on the ligand. The iridium center is pseudo-octahedral and the orbitals split into the usual d_{π} and $d\sigma^*$ levels, which would be t_{2g} and e_g in pure O_h symmetry. In these d^6 compounds the d_{π} orbitals are all filled in the ground state and include the HOMO, and the d-orbital ligand-field splitting is quite large on account of the substantial radial extension and strong metal-ligand overlap of the 5d orbitals. The d_{π} orbitals in these compounds

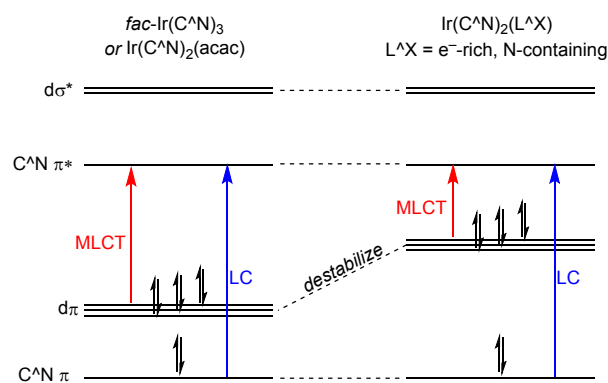


Fig. 3. Qualitative frontier orbital diagram for cyclometalated iridium complexes, showing the effect of incorporating and electron-rich ancillary ligand.

are not strictly localized on the metal and are best described as mixed metal-ligand orbitals, with major contribution from the C^N ligand aryl rings. Within the C^N ligands there are in reality several π and π^* orbitals that can participate in the low-energy excited states, but for simplicity Fig. 3 shows only a single energy level for each. These ligand-based frontier orbitals are localized on the C^N ligands in most $Ir(C^N)_3$ and $Ir(C^N)_2(L^AX)$ complexes, though it is very common for the π^* LUMO to localize on the ancillary ligand in $[Ir(C^N)_2(N^A)]^+$ complexes.

Also shown in Fig. 3 are the two major types of electronic transitions that dominate the low-energy excited states of these complexes. Within the C^N ligands there are $\pi \rightarrow \pi^*$ transitions possible, abbreviated here as "LC" for ligand-centered. The HOMO \rightarrow LUMO transition involves charge transfer from the d_{π} orbital to the $C^N \pi^*$, designating it as a metal-to-ligand charge transfer, MLCT. Given there are three d_{π} orbitals and many $C^N \pi$ and π^* orbitals, there are several LC and MLCT transitions that can be involved, but the simplified excited-state diagrams in Fig. 4 show one of each. The $^1\text{MLCT}$ state will be lower than the ^1LC , but because of the larger exchange interactions there is larger singlet-triplet splitting in the LC states, meaning the ^3LC state is normally the lowest-energy triplet state. The $^3\text{MLCT}$ state

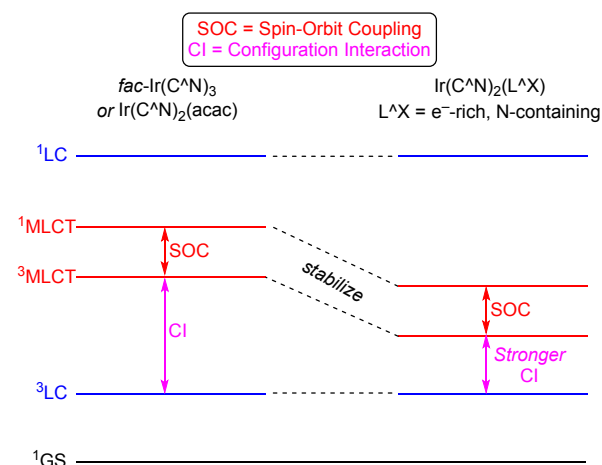


Fig. 4. Qualitative excited-state energy-level diagram, showing the effect of electron-rich ancillary ligands on triplet-state MLCT character and configuration interaction.

involves substantial spin-orbit coupling (SOC), and it mixes with the ^3LC state through configuration interaction, producing a luminescent low-energy triplet state (T_1) that is mixed $^3\text{LC}/^3\text{MLCT}$ character, with a small amount of $^1\text{MLCT}$ character from SOC. The degree of $^3\text{MLCT}$ character in T_1 is of critical importance to the excited-state dynamics. As shown in Equation 2, k_r also involves a square dependence on a spin-orbit coupling term, so states with larger SOC tend to have larger k_r values for $T_1 \rightarrow S_0$ radiative decay. Since all of the SOC derives from the MLCT states, T_1 states with higher MLCT character will have larger SOC and thus larger k_r values.

Other Metals Beyond Ir(III)

The focus of this article is our work on d^6 Ir(III) complexes, but we also point out that other metals have been explored in red to near-infrared phosphorescence, in particular d^8 Pt(II). The key difference between Ir(III) and Pt(II) complexes is that the latter adopt a square-planar geometry, resulting in a different d-orbital splitting pattern.^{1,6,28} Although the excited-state mixing in square-planar d^8 complexes is qualitatively similar to that described for iridium complexes in Fig. 5, in general square-planar platinum complexes have a weaker mixing of MLCT states than complexes with an octahedral geometry. Therefore, octahedrally coordinated complexes will show more efficient SOC than square-planar complexes. In support of this, phosphorescent cyclometalated platinum complexes typically have longer phosphorescence lifetimes and smaller zero-field splitting parameters compared to complexes of iridium(III) and osmium(II), two $5d$ metals which have octahedral geometries.¹ Nevertheless, the square-planar geometry of Pt(II) complexes can have some advantages, in particular the strong intermolecular Pt...Pt and π -stacking interactions that provide another layer of control over the photophysical properties, a feature which has been used advantageously in the design of efficient Pt-based NIR emitters which luminesce from excimeric states.^{29,30}

There are many examples of efficient red and near-infrared phosphorescence in other metals beyond iridium(III), and a few are highlighted here to give an idea of the breadth of discovery in this area. There is a review from 2013 which provides thorough coverage of near-infrared molecular phosphors,⁶ the general trend being that for complexes of most other d^6 metals NIR quantum yields are quite low. One notable exception is Os(II), which has triplet-state zero-field splitting values comparable to Ir(III)¹ and has been used in red to deep-red phosphors with good quantum yields.³¹ However, there has not been as extensive of development with osmium, likely due to toxicity concerns with this metal and its more limited coordination chemistry, centered around polypyridyl ligands with much fewer examples of cyclometalated complexes.^{32,33} Tridentate pincer-type ligands have emerged as a popular and effective choices for platinum phosphors which luminesce from monomeric, as opposed to excimeric or aggregated states. Chow et al. showed that extended π -conjugation on the pincer can engender red phosphorescence, albeit with modest quantum yields.³⁴ Improved platinum pincer complexes with efficient deep red to near-infrared phosphorescence were recently disclosed by the groups of Herbert and Williams,

supported by amido-based pincer ligands with flanking benzannulated N -heterocycle donors.^{35,36} Besides these well-studied systems, some recent advances have been made with Au(III) complexes, also typically supported by pincer ligands.³⁷ Au(III) derivatives have the same d^8 electron configuration and square-planar geometry as Pt(II), and some versions of these compounds can have red to NIR phosphorescence, with good quantum yields when doped into polymer films.³⁸

Synthetic Control of MLCT Character and SOC

At the heart of our strategy for optimizing the quantum yields of red to NIR phosphors is using ancillary ligand design to augment the excited-state MLCT character and SOC as a means of increasing k_r and Φ_{PL} . More specifically, we have pioneered the approach of using electron-rich, π -donating ancillary ligands, replacing the ubiquitous acac ligand, as a means of controlling these parameters. Fig. 3 and 4 also show how the ancillary ligand can influence frontier orbital and excited state energies. The ancillary ligand can have significant interactions with the $d\pi$ orbitals. The central hypothesis of our work is that electron-rich, π -donating, nitrogen-containing ancillary ligands will destabilize the $d\pi$ HOMO, as shown in the right side of Fig. 3. The orbitals associated with the C^N ligands are minimally perturbed, and though the effects on $d\pi^*$ are unclear these orbitals do not participate in the relevant excited states anyway. The consequence of this $d\pi$ perturbation on the excited-state manifold is a decrease in $^1/3\text{MLCT}$ energies, which then mix in more strongly with the ^3LC state through configuration interaction (see Fig. 4). This results in more MLCT character in the T_1 state, and thus larger SOC.

The effectiveness of the above strategy can depend on the choice of cyclometalating ligand. As outlined in Fig. 1, the cyclometalating ligands 2-pyridylbenzothiofene (btp) and 1-phenylisoquinoline (piq) are commonly used to engender red phosphorescence in cyclometalated iridium complexes, and we have used these extensively in the work we are highlighting here. Both btp and piq give similarly colored red phosphorescence in Ir(C^N)₂(acac) structures, and have both been used in top-performing OLED dopants (see Fig. 2), but their excited state character is markedly different. On the basis of experimental measurements of zero-field splitting, which correlate with the amount of MLCT character in the emissive state,¹ Ir(btp)₂(acac) has a primarily ^3LC excited state with MLCT perturbation,^{39,40} whereas the T_1 state in Ir(piq)₂(acac) is almost a pure $^3\text{MLCT}$ state.⁴¹ This pattern holds true for many other complexes with similar cyclometalating ligands, the key distinction being C^N ligands with thiophene-derived cyclometalated aryl rings resulting in predominant ^3LC character, and those with cyclometalated phenyl rings being mostly $^3\text{MLCT}$. The result of this difference is that, based on the arguments presented in Fig. 3 and 4, Ir(piq)₂(L^X) complexes should be more sensitive to changes in the L^X ligand. The L^X ligand primarily influences the MLCT states that dominate the emissive state when C^N = piq, so with electron-rich ancillary ligands the T_1 energy, the degree of SOC, and the magnitude of k_r can all be strongly influenced. When C^N = btp there is weaker configuration interaction between the $^3\text{MLCT}$ and ^3LC

states and T_1 is dominated by the latter, so perturbation of the MLCT states via ancillary ligand modification is likely to have more subtle influences on the photoluminescence.

For the remainder of this article, we describe how we have put the ideas described above into practice, using the inherent connections between ligand design and excited-state dynamics to guide our discovery of top-performing red to near-infrared phosphors. We have surveyed a number of compounds in the $\text{Ir}(\text{C}^{\wedge}\text{N})_2(\text{L}^{\wedge}\text{X})$ family, focusing primarily on complexes with $\text{C}^{\wedge}\text{N} = \text{ppy}$ and pbt , allowing us to make significant advances in the design of red ($\lambda_{\text{em}} \sim 600\text{--}650\text{ nm}$) and deep-red ($\lambda_{\text{em}} \sim 650\text{--}700\text{ nm}$) cyclometalated iridium phosphors. In our most recent work, we have extended into the NIR region, $\lambda_{\text{em}} > 700\text{ nm}$. Our ancillary ligand scope is varied in terms of donor atom combinations, chelate ring size, substituents, steric profile, and rigidity, allowing detailed structure-property relationships to be determined. The work we highlight here, all carried out within the past five years, reveals that electron-rich ancillary ligands are a powerful and previously overlooked design element for bis-cyclometalated iridium complexes with low-energy phosphorescence.

Ancillary ligand modification

Our group's earliest studies on bis-cyclometalated iridium complexes with electron-rich, nitrogen-containing ancillary ligands were not specifically focused on red to near-infrared phosphorescence. We initially prepared the compounds summarized in Fig. 5, where the cyclometalating ligand is either 2-phenylpyridine (ppy) or 2-phenylbenzothiazole (pbt), and the ancillary ligands were either β -ketoiminate (acNac) or β -diketiminate (NacNac), isoelectronic analogues of acac with increasing nitrogen content.⁴² Throughout this manuscript, we will use numbers to designate the cyclometalating ($\text{C}^{\wedge}\text{N}$) ligand in the $\text{Ir}(\text{C}^{\wedge}\text{N})_2(\text{L}^{\wedge}\text{X})$ complexes we discuss, with letters indicating the ancillary ligand. The $\text{Ir}(\text{ppy})_2(\text{L}^{\wedge}\text{X})$ (**1a–c**) and $\text{Ir}(\text{pbt})_2(\text{L}^{\wedge}\text{X})$ (**2a–c**) series gave us our initial insights into the electronic effects of the electron-rich ancillary ligands, as evaluated by cyclic voltammetry measurements. As summarized in Fig. 6, we observed very consistent trends in the

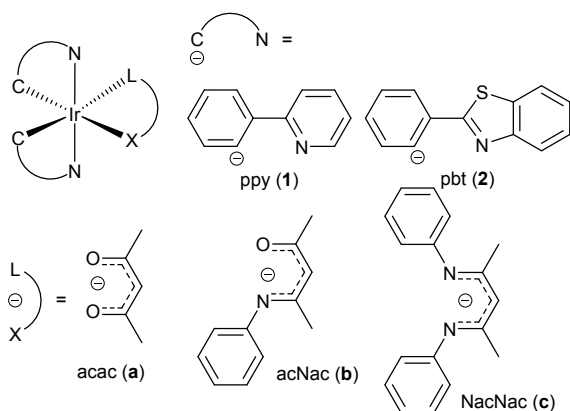


Fig. 5. Structures of the earliest examples of $\text{Ir}(\text{C}^{\wedge}\text{N})_2(\text{L}^{\wedge}\text{X})$ complexes with electron-rich, nitrogen-containing acNac and NacNac ancillary ligands.

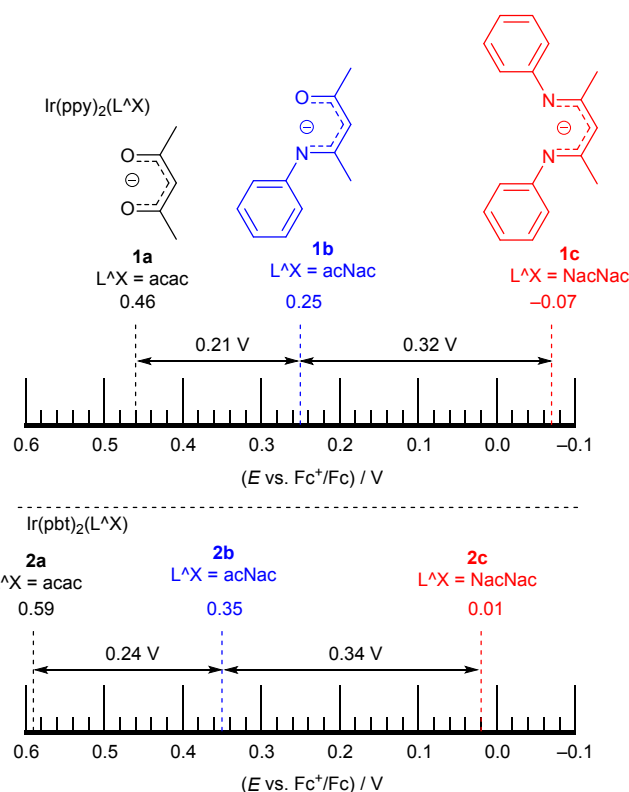


Fig. 6. Summary of the one-electron $\text{Ir}^{\text{IV}}/\text{Ir}^{\text{III}}$ redox potentials in $\text{Ir}(\text{ppy})_2(\text{L}^{\wedge}\text{X})$ (**1a–c**) and $\text{Ir}(\text{pbt})_2(\text{L}^{\wedge}\text{X})$ (**2a–c**) as a function of $\text{L}^{\wedge}\text{X}$ ligand.

$\text{Ir}^{\text{IV}}/\text{Ir}^{\text{III}}$ redox couple as a function of the ancillary ligand. We note a pronounced ca. 0.2 V cathodic shift upon replacing one oxygen donor in acac (**a**)¹⁶ with a nitrogen donor in acNac (**b**), and an additional ca. 0.3 V shift when moving from acNac (**b**) to NacNac (**c**). Although there are slight differences as a function of $\text{C}^{\wedge}\text{N}$ ligand, we see that this $\text{Ir}^{\text{IV}}/\text{Ir}^{\text{III}}$ potential is largely dictated by the $\text{L}^{\wedge}\text{X}$ ligand. In addition to the well-defined one-electron oxidation couple, the $\text{C}^{\wedge}\text{N} = \text{pbt}$ complexes (**2a–c**) have two reversible one-electron reduction waves, corresponding to population of a π^* LUMO on each of the pbt ligands. These potentials are largely independent of the ancillary ligand, varying by less than 0.1 V across the series. These electrochemical trends confirm the validity of the frontier orbital picture diagrammed in Fig. 3., whereby the addition of electron-rich ancillary ligands has a pronounced impact on the energy of the $d\pi$ HOMO, destabilizing it as the $\text{L}^{\wedge}\text{X}$ ligand is made more electron-rich, but has minimal impact on the energies of the unoccupied $\text{C}^{\wedge}\text{N}$ π^* orbitals. These trends in frontier orbital energies, clearly revealed in our earliest work on acNac and NacNac ancillary ligands, are preserved throughout the large set of compounds we describe in this paper. In addition, in work that is not described here in detail, we have shown that the electrochemical perturbations brought on by NacNac ancillary ligands are beneficial in photoredox applications, with complex **1c** and related derivatives emerging as state-of-the-art photoreductants for photoredox

transformations involving substrates that are difficult to reduce.^{43,44}

The compounds in this initial study, in particular the C^{^N} = pbt series **2a–c**, also provided some initial insights into the photophysical consequences of incorporating electron-rich ancillary ligands. The spectra and photoluminescence data are shown in Fig. 7. As can be seen from the spectra, the sequential incorporation of nitrogen donors into the ancillary ligand results in a progressive red shift of the PL maximum. In addition, the compound Ir(pbt)₂(acNac) (**2b**) has a substantially higher quantum yield than its acac counterpart (**2a**), 0.82 vs. 0.63. This large enhancement in Φ_{PL} is largely driven by a near doubling of the radiative rate constant, k_r , in **2b** vs. **2a**. In NacNac complex **2c** the quantum yield is substantially decreased, on account of a much larger k_{nr} value. These findings motivated us to explore whether these same design elements would be effective for red and near-infrared-emitting compounds. To better understand structure-property relationships and widen our search for state-of-the-art phosphors, our recent works on red-emitting complexes have moved beyond the acNac/NacNac families. We have focused on the effects of donor atom identity, chelate ring size, and substituents of the ancillary L^{^X} ligand on the electronic structure and excited state properties that can result in faster radiative rates and augmented quantum yields.

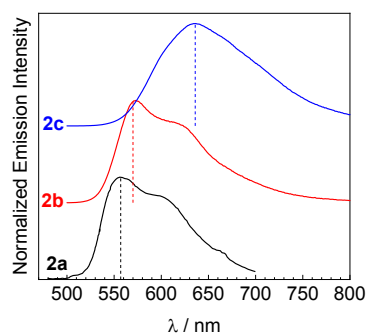
Red-emitting iridium complexes

As described in the Introduction, we have primarily used two different cyclometalating ligands, btp and piq, to support red-phosphorescent Ir(C^{^N})₂(L^{^X}) complexes. The structures of many of the compounds we have investigated in our work^{45–47} are summarized in Fig. 8. As before, we use numerical designators for each cyclometalating ligand, **3** for btp and **4** for piq, with letters to designate the different ancillary ligands. The L^{^X} ligands in this series are *N,O*-chelating β -ketoiminate (acNac), *N,N*-chelating β -diketiminato (NacNac), in addition to

smaller-bite angle ligands from the amidate (*N,O*), amidinate (*N,N*) and guanidinate (*N,N*) families. The study of these complexes shows different effects of changing the ancillary ligand on the emission.

The electrochemical effects of the electron-rich ancillary ligands are analogous to what we observed before in complexes with C^{^N} = ppy and btp (Fig. 6). The piq complexes show two reversible one-electron reduction waves beyond -2.0 V resulting from subsequent population of a π^* orbital on each C^{^N} ligand. Comparing the reduction potentials indicates that the identity of the ancillary ligands has little effect on the potentials.^{45–47} However, the Ir^{IV}/Ir^{III} potentials are once again highly dependent on the identity of the ancillary ligands, and in all cases the potentials for the compounds with nitrogen-containing ancillary ligands are cathodically shifted relative to the respective acac complex, indicating HOMO destabilization with the more electron-rich L^{^X} ligands. The effects of donor atoms in the acac/acNac/NacNac series^{45,48} are nearly identical to those shown in Fig. 6. Replacing one O with an *N*-phenyl group (**4a** to **4b**) results in a cathodic shift of 0.2 V, and a slightly larger shift of 0.3 V is observed by replacing the second O with *N*-phenyl (**4b** to **4c**), resulting in an overall 0.5 V cathodic shift compared to **4a**. A similar trend is also observed with smaller bite angle complexes **4f** (*N,O*-chelating amidate, $E(\text{Ir}^{\text{IV}}/\text{Ir}^{\text{III}}) = 0.42$ V) and **4d** (*N,N*-chelating amidinate, $E(\text{Ir}^{\text{IV}}/\text{Ir}^{\text{III}}) = 0.12$ V).⁴⁶ The effect of ancillary ligand chelate ring size on the oxidation potential can be noted by comparing a six-membered chelate complex with a four-member chelate complex, at parity of donor atoms. In all cases complexes with the smaller chelate ring size have more positive Ir^{IV}/Ir^{III} potentials, for example **4b** (6-member chelate acNac, +0.27 V) vs. **4e** (4-member chelate paa, +0.40 V), and **4c** (6-member chelate NacNac, -0.06 V) vs. **4d** (4-member chelate dipba, +0.12 V). This indicates that the smaller-bite-angle L^{^X} ligands have less of a destabilizing effect on the HOMO, which we believe is a result of poorer $d\pi$ angular overlap with the smaller chelating ligands. The electrochemical trends for the C^{^N} = btp complexes (**3**) follow a nearly identical trend, although only a single one-electron reduction is observed, often irreversible. Moreover, the cathodic shifts of the Ir^{IV}/Ir^{III} couples are not as pronounced, likely because the electron-rich benzothiophene contributes strongly to the HOMO and thus attenuates the effect of the ancillary ligand, but we still observe the general trend that increasing the ancillary ligand nitrogen content progressively destabilizes the HOMO.

We start our discussion of photoluminescence properties with the compounds that phosphoresce in the red region, defined here as having peak wavelengths between 600 and 650 nm. When C^{^N} = btp, the photoluminescence wavelength and excited-state dynamics are generally insensitive to the ancillary ligand structure, and all btp complexes we have prepared are red-phosphorescent. As shown in Fig. 9, the parent complex Ir(btp)₂(acac) (**3a**) luminesces with a peak wavelength of 612 nm and a quantum yield of 0.51.¹¹ Also shown in Fig. 9, the spectra of complexes **3b–j** with more electron-rich L^{^X} ligands are all quite similar, with peak emission wavelengths spanning a



	2a	2b	2c
λ / nm	557	570	636
Φ_{PL}	0.63	0.82	0.21
$\tau / \mu\text{s}$	1.8	1.2	0.61
k_r / s^{-1}	3.5×10^5	6.8×10^5	3.4×10^5
$k_{\text{nr}} / \text{s}^{-1}$	2.1×10^5	1.5×10^5	1.3×10^6

Fig. 7. Summary of photoluminescence data for complexes **2a–c**, recorded at room temperature in 2-methyltetrahydrofuran (**2a**) or tetrahydrofuran (**2b** and **2c**). The dashed lines in the spectra show the peak wavelength for each compound, to help visualize the differences between them. The spectrum for **2a** is adapted with permission from reference 16. Copyright 2001 American Chemical Society.

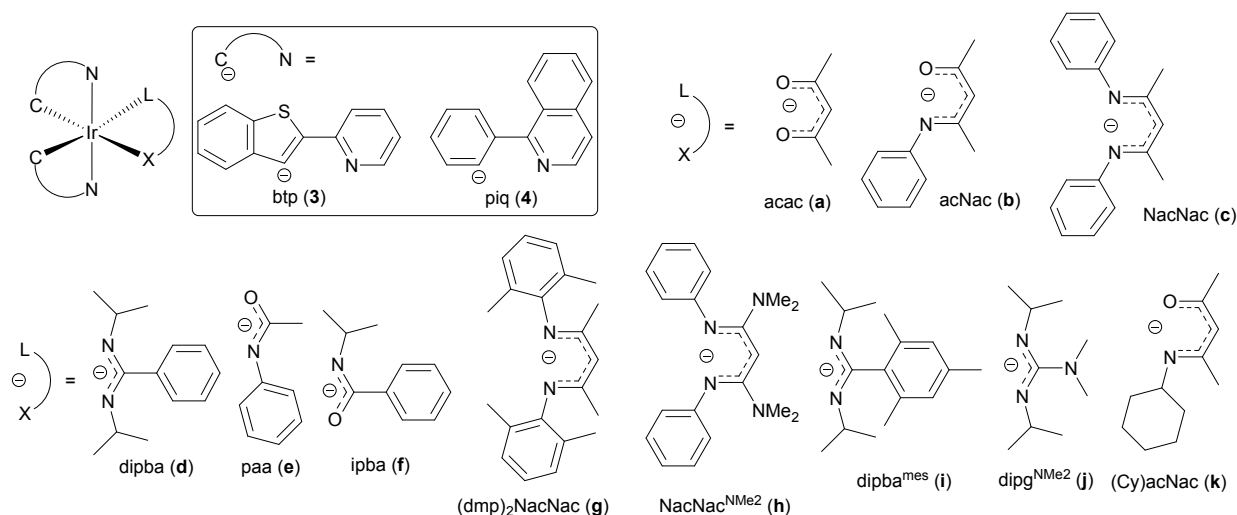
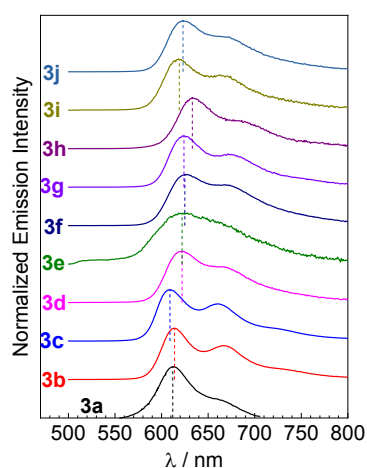


Fig. 8. Structures of red and deep-red phosphorescent $\text{Ir}(\text{btp})_2(\text{L}^{\wedge}\text{X})$ (**3**) and $\text{Ir}(\text{piq})_2(\text{L}^{\wedge}\text{X})$ (**4**) complexes.



	3a ¹¹	3b	3d	3f
λ / nm	612	614	622	625
Φ_{PL}	0.51	0.33	0.79	0.34
$\tau / \mu\text{s}$	5.8	5.8	5.3	5.1
k_r / s^{-1}	8.8×10^4	5.7×10^4	1.5×10^5	6.6×10^4
$k_{\text{nr}} / \text{s}^{-1}$	8.4×10^4	1.2×10^5	4.0×10^4	1.3×10^5

Fig. 9. Summary of photoluminescence data for complexes **3a–j**, recorded at room temperature in 2-methyltetrahydrofuran (**3a**) or tetrahydrofuran (**3b–j**). The dashed lines in the spectra show the peak wavelength for each compound, to help visualize the differences between them. The spectrum for **3a** is adapted with permission from reference 11. Copyright 2001 American Chemical Society. The data table summarizes the four complexes in the series with the highest photoluminescence quantum yields; complete data for the rest can be found in our previous publications.^{45–47}

narrow range of 609–633 nm in these compounds.^{45–47} Furthermore, for most members in this series the photoluminescence quantum yields are ~ 0.2 – 0.3 , slightly lower than **3a**. Some of the more electron-rich ancillary ligands, like $(\text{dmp})_2\text{NacNac}$ (**3g**), $\text{NacNac}^{\text{NMe}_2}$ (**3h**), and $\text{dipg}^{\text{NMe}_2}$ (**3j**) have a moderate effect on the excited-state energy, with peak wavelengths that are bathochromically shifted by 300–500 cm^{-1} relative to **3a**, but even in these compounds the excited-state dynamics, in particular k_r , are all quite similar to the parent acac

complex. However, a notable exception is observed with $\text{Ir}(\text{btp})_2(\text{dipba})$ (**3d**), which exhibits a modest red shift in the emission maximum relative to $\text{L}^{\wedge}\text{X} = \text{acac}$ ($\lambda_{\text{em}} = 622$ vs. 612 nm) and a large increase in k_r and photoluminescence quantum yield ($\Phi_{\text{PL}} = 0.79$) compared to the other members of the series.⁴⁵ More specifically, the k_r value in **3d** is $1.5 \times 10^5 \text{ s}^{-1}$, nearly double that of acac complex **3a** ($8.8 \times 10^4 \text{ s}^{-1}$). This complex represents one of the most efficient red phosphors ever discovered, surpassing the quantum yields of the compounds that have been doped into the most efficient red OLED devices (Fig. 2).

At this point it is not entirely clear why the dipba ancillary ligand in **3d** is uniquely effective at engendering efficient red phosphorescence in the $\text{Ir}(\text{btp})_2(\text{L}^{\wedge}\text{X})$ series. To explain the general lack of sensitivity of these compounds to the ancillary ligand identity, we refer back to Fig. 3 and 4 in the Introduction. In these $\text{Ir}(\text{btp})_2(\text{L}^{\wedge}\text{X})$ compounds the well-resolved vibronic structure (Fig. 9), moderately long lifetimes (~ 3 – $6 \mu\text{s}$ for most compounds), and in the parent $\text{Ir}(\text{btp})_2(\text{acac})$ compound (**3a**) the moderate zero-field splitting (ZFS)^{39,40} are all hallmarks of luminescence from primarily a ^3LC state, perturbed slightly by mixing with $^1,^3\text{MLCT}$. In other words, configuration interaction between the ^3LC and $^3\text{MLCT}$ states in these compounds is comparatively weak. Thus, even though the electron-rich $\text{L}^{\wedge}\text{X}$ ligands in **3b–j** destabilize the HOMO, reduce the HOMO–LUMO gap, and stabilize the MLCT states, in general there is still relatively little MLCT character in the emissive state, so these perturbations have only subtle impacts on the energy and dynamics of the T_1 state. Nevertheless, in amidinate complex **3d** the slight red-shift, broader spectral profile, and augmented k_r value are all characteristic of increased MLCT character. This increase in k_r is coupled with fortuitously small k_{nr} value ($4.0 \times 10^4 \text{ s}^{-1}$) that is $>2\times$ smaller than any of the other $\text{Ir}(\text{btp})_2(\text{L}^{\wedge}\text{X})$ compounds, leading to the impressively high solution Φ_{PL} of 0.79.

In contrast, the $\text{Ir}(\text{piq})_2(\text{L}^{\wedge}\text{X})$ complexes have photoluminescence spectra and excited-state dynamics that are very responsive to the nature of the ancillary ligand. This

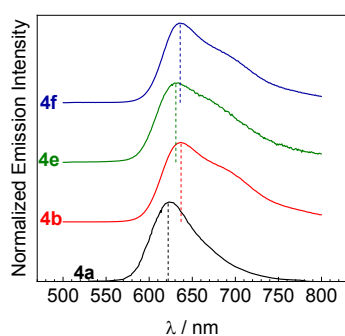
difference arises because the nature of the excited state is altered when $C^{\wedge}N = \text{piq}$. On the basis of their large zero-field splitting values, the triplet states of *fac*-Ir(piq)₃⁴⁹ and Ir(piq)₂(acac) (**4a**)⁴¹ are classified as predominantly MLCT.¹ In addition, as will be seen throughout this section, the radiative rate constants in complexes with $C^{\wedge}N = \text{piq}$ are almost one order of magnitude higher than those with $C^{\wedge}N = \text{bt}$, also consistent with augmented MLCT character. As a result, perturbations to the ancillary ligand, which can have a large effect on $d\pi$ HOMO (Fig. 3) and MLCT (Fig. 4) energies, are expected to substantially impact both the energy and the dynamics of the T₁ state. The new complexes we have prepared are compared with a reference compound Ir(piq)₂(acac) (**4a**) that has an emission maximum at 622 nm.⁵⁰ A noticeable effect on the emission maximum is observed by substituting acac to nitrogen-containing ancillary ligands. Substitution of one ancillary oxygen donor with *N*-Ph, Ir(piq)₂(acNac) (**4b**), results in a 400 cm⁻¹ bathochromic shift of the emission maximum to 637 nm. Replacing both ancillary oxygen donors with nitrogens, for example Ir(piq)₂(NacNac) (**4c**) and Ir(piq)₂(dipba) (**4d**), has a more significant effect on the emission maximum which appear at 678 nm (**4c**) and 671 nm (**4d**), a >1100 cm⁻¹ red shift relative to Ir(piq)₂(acac).⁴⁵ In addition, a loss of vibronic structure is observed as additional nitrogen donors are incorporated in the ancillary ligand, suggesting an increase in excited-state charge-transfer character as more electron-rich ancillary ligands are incorporated.

As a result of high sensitivity of the photoluminescence wavelength to the ancillary ligand structure, only the Ir(piq)₂(L[^]X) complexes with *N,O*-chelating ancillary ligands (acNac (**4b**), paa (**4e**), and ipba (**4f**), see Fig. 8) luminesce in the red region, i.e. with peak wavelengths between 600 and 650 nm.^{45,46} The spectra of these complexes, along with the reference compound Ir(piq)₂(acac) (**4a**) are shown in Fig. 10. The

three complexes with nitrogen-containing ancillary ligands all have spectra that are moderately red-shifted from that of **4a**, by ~200–400 cm⁻¹. Quantum yields and emission lifetimes also showed the effect of the ancillary ligand on the excited-state dynamics. Replacing acac (**4a**) with acNac (**4b**) results in a ca. 7-fold increase in the radiative rate constant (k_r) from $1.2 \times 10^5 \text{ s}^{-1}$ to $8.0 \times 10^5 \text{ s}^{-1}$ with a small decrease in the nonradiative rate constant (k_{nr}). This leads to an increase in the quantum yield (Φ_{PL}) from 0.20 to 0.80, which is also significantly higher than that of *fac*-Ir(piq)₃ ($\Phi_{\text{PL}} = 0.53$, Fig. 2).^{24,49} The smaller bite-angle amidate ancillary ligands are not as beneficial to the excited state dynamics. The large k_{nr} in *N*-phenylacetamide complex **4e** results in a lower quantum yield (0.12), whereas in *N*-isopropylbenzamidate complex **4d** there is a sizeable increase in k_r that contributes to a significant augmentation of Φ_{PL} to 0.47, albeit not as dramatic as the increase observed in **4b** with acNac. The larger effects observed with the larger bite-angle acNac are likely again related to the stronger angular overlap with the $d\pi$ orbitals. Via the mechanism outlined in Fig. 3 and 4, the larger bite-angle ligand is more effective at perturbing the energies of the $d\pi$ orbitals, which leads to more MLCT character in T₁ and a faster radiative decay rate. We have also investigated two pyridyl-based L[^]X ligands, 2-(2-pyridyl)indolate and 2-(2-pyridyl)phenolate, which result in red luminescence when coordinated to [Ir(piq)₂]⁺.⁴⁶ For the sake of cohesiveness we will not discuss these two other structural classes in detail and will focus only on the π -delocalized monoanionic chelates shown in Fig. 8, but we do note that the latter 2-(2-pyridyl)phenolate complex had a very good quantum yield of 0.54 with a peak wavelength of 638 nm.

To summarize our advances in the design of red-phosphorescent cyclometalated iridium complexes, we have discovered two complementary structures, Ir(btp)₂(dipba) (**3d**) and Ir(piq)₂(acNac) (**4b**), with record-breaking photoluminescence quantum yields in the red region, both near 80%. As our part of our efforts in this area we investigated almost a dozen Ir(btp)₂(L[^]X) structures, and found that with this cyclometalating ligand the photoluminescence spectra and excited-state dynamics are generally insensitive to the structure of the ancillary ligand, as a result of the primarily ³LC emissive state. As such, all of these compounds luminesce in the red region and most have very similar quantum yields, excepting amidinate complex **3d** as a noteworthy outlier. In the Ir(piq)₂(L[^]X) series the triplet excited state is primarily MLCT and is thus very responsive to the structure of the ancillary ligand. Most complexes with *N,O*-chelating ancillary ligands luminesce in the red region, and all have larger k_r values than the reference compound Ir(piq)₂(acac). With more electron-rich *N,N*-chelating ancillary ligands, the photoluminescence maxima of Ir(piq)₂(L[^]X) complexes shift into the deep red region, beyond 650 nm. In the next section we will summarize our efforts to optimize the photoluminescence spectra of these deep-red phosphors, where again judicious choice of ancillary ligand is critical.

Deep-red emitting iridium complexes



	4a ⁵⁰	4b	4e	4f
λ / nm	622	637	631	636
Φ_{PL}	0.2	0.80	0.12	0.47
$\tau / \mu\text{s}$	1.7	1.0	0.55	0.99
k_r / s^{-1}	1.2×10^5	8.0×10^5	2.2×10^5	4.7×10^5
k_{nr} / s^{-1}	4.8×10^5	2.0×10^5	1.6×10^6	5.3×10^5

Fig. 10. Summary of photoluminescence data for red-phosphorescent Ir(piq)₂(L[^]X) complexes **4a**, **4b**, **4e**, and **4f**, recorded at room temperature in dichloromethane (**4a**) or tetrahydrofuran (**4b**, **4e**, and **4f**). The dashed lines in the spectra show the peak wavelength for each compound, to help visualize the differences between them. The spectrum for **4a** is adapted with permission from reference 50. Copyright 2003 John Wiley and Sons.

In some of our earliest work on red-phosphorescent complexes, we described the complexes Ir(piq)₂(NacNac) (**4c**) and Ir(piq)₂(dipba) (**4d**) (see Fig. 8).⁴⁵ We found that these two deep-red emitters, $\lambda_{\text{em}} = 678 \text{ nm}$ (**4c**) and 671 nm (**4d**), have smaller k_r values and larger k_{nr} values than the red-phosphorescent compounds described above, limiting their quantum yields to values of 0.17 (**4c**) and 0.34 (**4d**). These results were nevertheless encouraging, since these quantum yields are still reasonably high for phosphorescence that deep in the red region. Building off our initial study, we then modified the ancillary ligands to improve deep-red-emitting cyclometalated iridium complexes.⁴⁷ To reach our goal, we introduced modifications to the ancillary ligand designed to make it more sterically encumbered or more electron-rich (Fig. 8). We hypothesized that with more sterically encumbered ancillary ligands we could suppress k_{nr} as a means of improving the quantum yield, and with more electron-rich ancillary ligands we could shift the luminescence deeper into the red, possibly into the near-infrared region. We introduced methyl substituents at the ortho positions of the N-aryl groups in (dmp)₂NacNac (**4g**) to increase the steric profile. Also, to make the NacNac ancillary ligand more electron-rich we added dimethylamino substituents to the backbone (NacNac^{NMe₂}, **4h**), and for acNac we replaced the N-phenyl substituent with a cyclohexyl ring in (Cy)acNac (**4k**). Similarly, we modified the amidinate to make it more sterically encumbered (dipba^{mes}, **4i**), or more electron-rich by changing to a guanidinate (dipg^{NMe₂}, **4j**).

Most of these same ancillary ligands were used in Ir(btp)₂(L^{AX}) complexes (**3a–j**), which all luminesce in the red region as shown in Fig. 9. However, in the Ir(piq)₂(L^{AX}) series with these more electron-rich ancillary ligands the emission maxima of the complexes occur beyond 650 nm in the deep red region of the spectrum and are responsive to the ancillary ligand structure, as shown in Fig. 11. To better visualize the effects of the ancillary ligand structure on these compounds, Fig. 12 shows the consequences of either rigidifying the ancillary ligand or making it even more electron rich. Making the ancillary ligand more electron-rich red-shifts the photoluminescence, offering a potential strategy for preparing near-infrared phosphors.

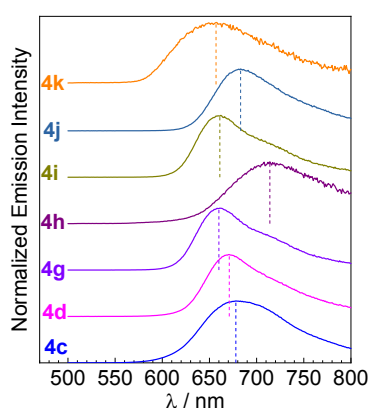


Fig. 11. Summary of photoluminescence data for deep red-phosphorescent Ir(piq)₂(L^{AX}) complexes **4c**, **4d**, and **4g–k**, recorded at room temperature in tetrahydrofuran. The dashed lines in the spectra show the peak wavelength for each compound, to help visualize the differences between them.

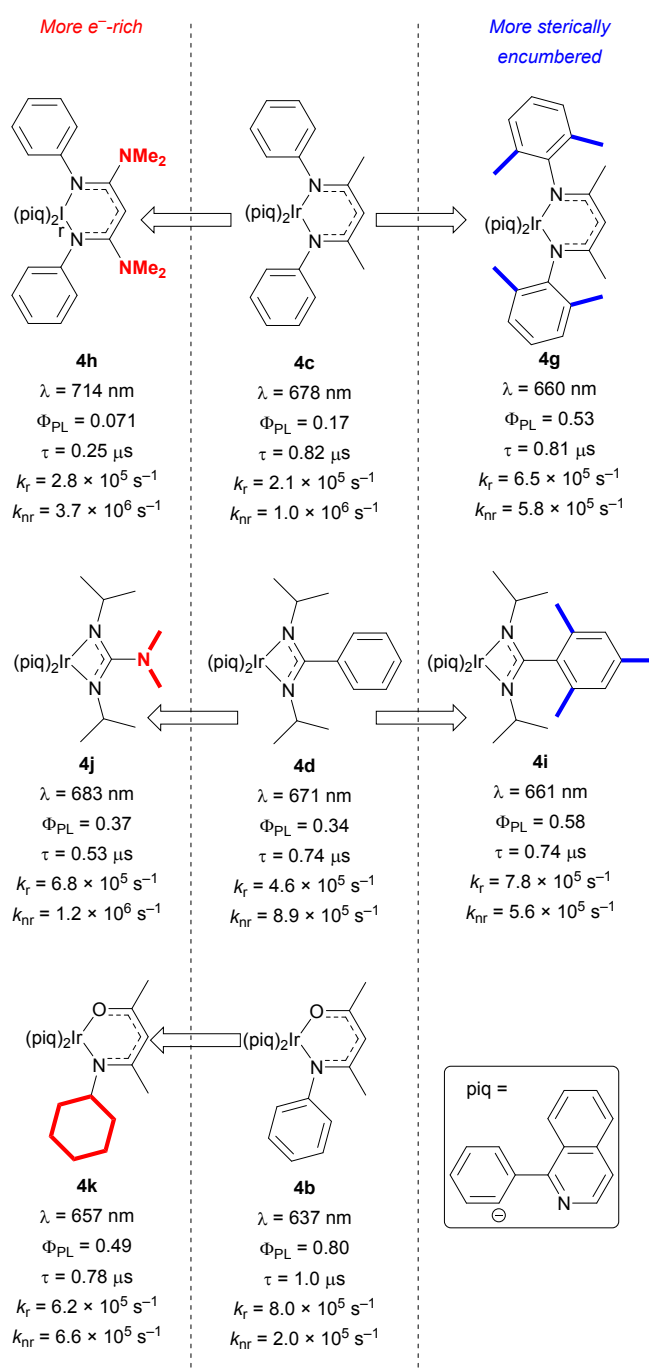


Fig. 12. Summary of the effects of ancillary ligand modification on the photoluminescence and excited-state dynamics of deep-red Ir(piq)₂(L^{AX}) complexes.

Starting with dipba complex **4d**, substituting the backbone phenyl ring with a dimethylamino group in dipg^{NMe₂} complex **4j** results in a modest 12-nm (260 cm⁻¹) bathochromic shift in photoluminescence maximum, which shifts from 671 nm to 683 nm while maintaining a nearly identical quantum yield (0.34 in **4d**, 0.37 in **4j**). The dimethylamino substituents in NacNac^{NMe₂} complex **4h** are more effective at red-shifting the photoluminescence maximum, which is perturbed from 678 nm in unsubstituted complex **4c** to 714 nm in **4h**, a difference of 740 cm⁻¹. The photoluminescence in **4h** can be characterized as

near-infrared, however, in this case the bathochromic shift occurs at the expense of efficiency, with the quantum yield decreasing from 0.17 in **4c** to 0.071 in **4h**, suggesting that using extremely electron-rich ancillary ligands to target NIR phosphorescence may not be an effective strategy. As one final example, (Cy)acNac complex **4k** that incorporates an *N*-alkyl substituent onto the β -ketoiminate is also an effective design for deep-red luminescence, exhibiting a λ_{em} of 657 nm and a quantum yield of 0.49. The photoluminescence in **4k** is red-shifted by 480 cm^{-1} relative to parent acNac complex **4b** (see Fig. 9), and while the quantum yield isn't as high it is still one of the highest ever for deep-red phosphorescence.

Figure 12 also shows the effects of rigidifying the ancillary ligand, which can have profound impacts on the excited-state dynamics.⁴⁷ Two illustrations of these effects are found in compounds **4g** and **4i**, more sterically crowded analogues of **4c** and **4d**. Compared to NacNac compound **4c** that has a photoluminescence λ_{em} of 678 nm and a Φ_{PL} of 0.17, we observe a blue shift in **4g** to 660 nm, but a significant increase in quantum yield to 0.53. A similar trend is observed with dipba compound **4d** and its more sterically crowded analogue **4i**. In line with our hypothesis the increases in quantum yield are to some extent due to a decrease in k_{nr} , about 40% in both cases, but an unexpected result is that the more structurally rigid analogues **4g** and **4i** also exhibited larger radiative rate constants (k_r) by a factor of 3.1 (**4c** to **4g**) and 1.7 (**4d** to **4i**). Thus, both an increase in k_r and a decrease in k_{nr} led to the higher quantum yields in sterically encumbered complexes. We hypothesize that the slight blue-shift in complexes **4g** and **4i** is a result of the more sterically crowded ancillary ligand leading to a less distorted T_1 state, reducing the singlet-triplet gap.

Taken together, these results not only unveiled several structure-property relationships, but also led to the discovery of a few top-performing deep-red phosphors that are significantly more efficient than previous analogues. We demonstrated three compounds – **4g**, **4i**, and **4k** – that have photoluminescence maxima beyond 650 nm and quantum yields of 0.49 or greater. Moreover, dipbg^{NMe2} complex **4j** luminesces very deep in the red ($\lambda_{em} = 683\text{ nm}$) with a respectable quantum yield of 0.37. These $\text{Ir}(\text{piq})_2(\text{L}^{\wedge}\text{X})$ compounds all have higher quantum yields than some of the best-known deep-red phosphorescent iridium compounds in the literature, most of which are $\text{Ir}(\text{C}^{\wedge}\text{N})_2(\text{L}^{\wedge}\text{X})$ structures with highly conjugated $\text{C}^{\wedge}\text{N}$ ligands and acac or picolinate ancillary ligands.^{51–54} Preparing efficient deep-red iridium phosphors has been drawing attention for applications in optoelectronic devices, and the compounds shown here offer a complementary and effective approach to access deep-red emitters.

Near-infrared emitting iridium complexes

A typical way to engender near-infrared luminescence in cyclometalated iridium complexes is to use highly conjugated cyclometalating ligands to lower the triplet state (T_1) energy, often with acetylacetonate (acac) or bipyridine derivatives as ancillary ligands in bis-cyclometalated structures.^{55–57} As we described throughout this article, in red and deep-red

phosphorescent complexes electron-rich, π -donating ancillary ligands strongly perturb the metal-centered HOMO, increase the metal d-orbital participation in the excited state, and as a result augment k_r and Φ_{PL} . Expecting to see a similar trend in the near-infrared region, we designed new neutral near-infrared phosphorescent iridium complexes⁵⁸ with a phenanthridinebenzothiophene (btph) cyclometalating ligand, previously used in several other NIR cyclometalated iridium complexes.^{59–62} For our work in the red and deep red regions, we primarily used the β -ketoiminate, β -diketiminate, amidinate and amidate families as ancillary ligands (see Fig. 8), which in many cases had noticeable effects on k_r , but gave a little control over k_{nr} in general. Moreover, the cyclometalating ligand btph is a π -extended analogue of btp, and we showed in a large suite of $\text{Ir}(\text{btp})_2(\text{L}^{\wedge}\text{X})$ complexes (Fig. 9) that these ancillary ligand classes only in rare cases have beneficial impacts on the excited-state dynamics when $\text{C}^{\wedge}\text{N} = \text{btp}$. With this in mind, and cognizant of the importance of minimizing k_{nr} when designing NIR phosphors, we investigated a different ancillary ligand design for our first foray into NIR luminescence. We combined strong donor moieties on the ancillary ligand with a rigid fused aromatic skeleton, which could potentially suppress k_{nr} and augment the quantum yields of NIR phosphors. We reasoned that 8-substituted quinolines and 10-substituted benzoquinolines, some of which had been used to support visible-phosphorescent cyclometalated iridium complexes,^{63–65} could be good supporting ligands for NIR emitters. We formulated $\text{Ir}(\text{btph})_2(\text{L}^{\wedge}\text{X})$ complexes with 8-hydroxyquinoline (8OQ, **5l**), 8-carboxyquinoline (8COOQ, **5m**), 10-hydroxybenzo[h]quinoline (10OBQ, **5n**), 8-(1H-pyrrol-2-yl)quinoline (8PyQ, **5o**) and *N*-phenyl-8-quinolinecarboxamide (8CONPhQ, **5p**) as the ancillary ligands (Fig. 13).

PL spectra for complexes $\text{Ir}(\text{btph})_2(\text{acac})$ (**5a**) and quinoline-derived complexes **5l–p** are shown in Fig. 14. Much like the red-emitting $\text{Ir}(\text{btp})_2(\text{L}^{\wedge}\text{X})$ complexes described above (Fig. 9), the photoluminescence properties of these compounds are only

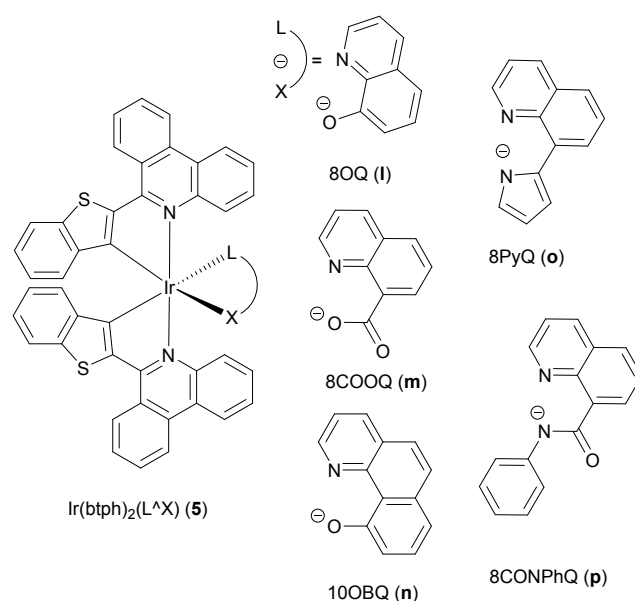
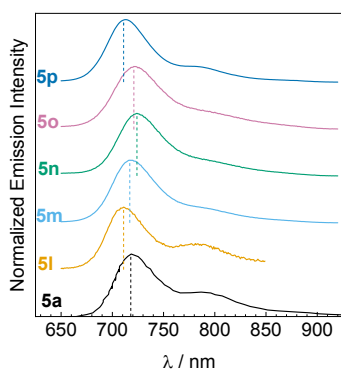


Fig. 13. Structures of NIR-emitting $\text{Ir}(\text{btph})_2(\text{L}^{\wedge}\text{X})$ complexes.



	5a ⁶¹	5l	5m
λ / nm	718	711	717
Φ_{PL}	0.28	0.36	0.30
$\tau / \mu\text{s}$	1.9	2.0	1.7
k_r / s^{-1}	1.5×10^5	1.8×10^5	1.8×10^5
$k_{\text{nr}} / \text{s}^{-1}$	3.8×10^5	3.2×10^5	4.1×10^6

	5n	5o	5p
λ / nm	724	721	713
Φ_{PL}	0.28	0.042	0.34
$\tau / \mu\text{s}$	1.5	1.0	1.6
k_r / s^{-1}	1.9×10^5	4.2×10^4	2.1×10^5
$k_{\text{nr}} / \text{s}^{-1}$	4.8×10^5	9.6×10^5	4.1×10^5

Fig. 14. Summary of photoluminescence data for NIR-phosphorescent Ir(btph)₂(L^X) complexes **5a** and **5l–p**, recorded at room temperature in tetrahydrofuran. The dashed lines in the spectra show the peak wavelength for each compound, to help visualize the differences between them. The spectrum for **5a** is adapted with permission from reference 61. Copyright 2015 Elsevier.

subtly responsive to the ancillary ligand. The emission maxima are in the NIR region ranging from 711 to 724 nm, with the 10OBQ complex **2n** having the largest red shift of 6 nm (120 cm^{-1}) and the hydroxyl complex **2k** showing the largest blue-shift of 7 nm (140 cm^{-1}) compared to the peak emission wavelength of Ir(btph)₂(acac) ($\lambda_{\text{max}} = 718 \text{ nm}$).⁶¹ The PL decays are all single exponential with lifetimes ranging from 1.0 to 2.0 μs , similar to Ir(btph)₂(acac) that has a lifetime of 1.9 μs .⁶¹ The photoluminescence quantum yields (Φ_{PL}) of most of the complexes are between 0.28 and 0.36, similar to or slightly higher than the reference complex Ir(btph)₂(acac) ($\Phi_{\text{PL}} = 0.28$).²⁹ One exception is observed in complex **2o** where $\Phi_{\text{PL}} = 0.042$, having more than four-fold smaller k_r and more than two-fold larger k_{nr} than the other complexes. The rest of the compounds with higher quantum yields have smaller k_{nr} values than most other structurally related deep-red and NIR phosphorescent compounds,^{47,56,66} which indicates that the rigidity of the btph C^N ligands and quinoline-based ancillary ligands combine to inhibit vibrational relaxation pathways. The most efficient emitter in this series is complex **2l** ($\Phi_{\text{PL}} = 0.36$) that has a slightly larger k_r and slightly smaller k_{nr} than Ir(btph)₂(acac) (**5a**), resulting in the increase in quantum yield. One trend found in **2l**, **2m**, **2n** and **2p**, where the quantum yields are equal to or slightly larger than Ir(btph)₂(acac), is that k_r values are slightly larger likely due to the more electron-rich donors in the ancillary ligands, which augments k_r as described in Fig. 3 and 4 and Equation 2. In most of the complexes, the PL dynamics are quite similar to one another and to Ir(btph)₂(acac), indicating

that the ancillary ligand does not generally have a large influence on the radiative and nonradiative decay from the triplet state. Among the five prepared bis-cyclometalated iridium near-infrared phosphorescent emitters, four of them have intense NIR emission with photoluminescence quantum yields that rival or exceed state-of-the-art NIR phosphors. This demonstrates that combining the rigid btph cyclometalating ligands with substituted quinoline ancillary ligands is an effective strategy for narrow and intense NIR emission, albeit with only modest improvements in k_r over the previously studied Ir(btph)₂(acac). This work again shows that in complexes where the cyclometalating ligand has an electron-rich thiophene ring, the excited state has more ³LC character and is in general less influenced by the ancillary ligands.

Outlook and future progress

The work described here introduces a fundamentally new approach for synthetically controlling the excited-state dynamics of bis-cyclometalated iridium complexes which phosphoresce in the low-energy regions of the spectrum. We have certainly developed a strong empirical understanding of the structure-property relationships we have uncovered, and some experimental insight into the effects of the electron-rich ancillary ligands on the frontier orbital energies and excited-state character. However, a much deeper experimental and theoretical understanding would certainly advance this work and strengthen the overarching messages. While our work suggests that increased excited-state MLCT character and larger spin-orbit coupling is largely responsible for the effects we see, more in-depth experimental and theoretical interrogation of the excited states would bolster or modify these conclusions. Ground-state DFT calculations⁴⁵ reveal that the HOMO in the Ir(piq)(L^X) series (**4a–d**; L^X = acac, acNac, NacNac, dipba) has increasing ancillary ligand character as the L^X ligand nitrogen content increases. This suggests that the HOMO→LUMO transition has substantial ligand-to-ligand charge transfer (LL'CT) character, but at this point our theoretical work is not yet at the level to reveal whether this HOMO composition is in fact important to the nature of the T₁ state, and whether LL'CT state(s) do contribute substantially to T₁ when the ancillary ligand is electron-rich. Experimentally, we have only collected emission spectra as low as 77 K, which provides further support of our conclusion that electron-rich ancillary ligands increase excited-state charge transfer character. In principle, although technically very challenging, luminescence measurements at liquid He temperatures ($\sim 4 \text{ K}$) in appropriate matrices¹ provide direct measures of the T₁ ZFS, which would allow us to determine whether increased SOC is in fact responsible for the larger k_r values we often observe in our compounds.

Whereas a deeper theoretical understanding of the triplet excited state in our compounds would benefit the entirety of our work, from a more tangible standpoint we think the immediate developments in our work, and a critical need in the field, is the continued improvement of NIR phosphors. The NIR will likely never receive as much attention as the visible region, since unlike visible phosphors there are not any commercial

applications that are as lucrative as colour displays, but there still remain fundamental challenges in NIR phosphor design and improved metrics could be beneficial to certain technologies, including but not limited to night-vision apparatuses and medical imaging devices. There have been some promising recent developments in NIR phosphors with other metals, like platinum,^{35,36} but we do think the underlying principles of the red and deep-red bis-cyclometalated iridium complexes we have studied are applicable to the NIR, and that the molecules can be appropriately tuned to realize even larger enhancements in NIR quantum yields. In our initial work in the NIR we used the cyclometalating ligand btph and rigid quinoline-based ancillary ligands, which were effective but afforded us only subtle control over the excited-state dynamics. Using our past work as a guide, we need to determine which combinations of cyclometalating and ancillary ligand are most suitable for NIR emission with high quantum yields. In future NIR designs we will either need to come up with ancillary ligands that are more effective at changing the nature of the triplet state in $\text{Ir}(\text{btph})_2(\text{L}^\wedge\text{X})$ complexes, or more feasibly, move to other classes of cyclometalating ligands which result in more excited-state MLCT character, which can then be more readily modulated by the ancillary ligand. Analogues of piq with extended conjugation and/or strategically placed substituents should suit these purposes and will be the focus of some of our next-generation NIR phosphors, paired with the types of electron-rich ancillary ligands described throughout this work. Our initial NIR targets all have peak λ_{em} values that are near 700 nm, but there are elaborately conjugated cyclometalating ligands that engender NIR luminescence even deeper in the spectrum, beyond 800–900 nm. We think this region of the spectrum is also ripe for future development and will be impacted down the line by the molecular design principles we have discovered.

Finally, it is worth noting that our work on $\text{Ir}(\text{C}^\wedge\text{N})_2(\text{L}^\wedge\text{X})$ complexes supported by electron-rich ancillary ligands has applications beyond red to NIR phosphorescence. We^{43,44} and others⁶⁷ have shown that electron-rich ancillary ligands can give rise to complexes which are very effective as visible-light photosensitizers, in particular functioning as strong photoreductants for photoredox catalysis. Although the cyclometalating ligands used for these applications are different, the synthetic and electronic-structure insights gained from the two thrusts are complementary. Thus, knowledge we have gained from our work in the red to NIR region may prove beneficial to photosensitizer designs for photoredox catalysis, and vice versa. For example, the ligands $(\text{dmp})_2\text{NaCNac}$ (**g**), $\text{NaCNac}^{\text{NMe}_2}$ (**h**), and $(\text{Cy})\text{acNac}$ (**k**) were all used originally in our group's research on photosensitizers,⁴⁴ but they have also proven to be insightful and, in two of the three cases, very effective supporting ligands for deep-red phosphorescence.⁴⁷ Thus, we believe that the progress we will make in the area of red to NIR phosphorescence may also be beneficial to the continued search for improved photosensitizers for photoredox catalysis.

Conclusions

We have introduced a new strategy for synthetic control of excited-state dynamics in red ($\lambda_{\text{em}} \sim 600\text{--}650$ nm), deep-red ($\lambda_{\text{em}} \sim 650\text{--}700$ nm), and near-infrared ($\lambda_{\text{em}} > 700$ nm) bis-cyclometalated iridium phosphors. Whereas there have been considerable previous efforts designing complexes which luminesce in these ranges, in particular the red region which has technological relevance in OLED displays, almost all previous designs were either from the $\text{Ir}(\text{C}^\wedge\text{N})_3$ or $\text{Ir}(\text{C}^\wedge\text{N})_2(\text{acac})$ structure types. Little attention had previously been paid to the influence of the ancillary ligand on the excited-state dynamics, and our work shows that electron-rich, nitrogen-containing monoanionic ancillary ligands, in many cases derived from acac, can have beneficial impacts on the photoluminescence attributes of red to NIR phosphors. This is especially true when the cyclometalated aryl group is a phenyl ring, as is the case with piq. In these complexes, all our experimental evidence from cyclic voltammetry and photoluminescence experiments is consistent with the idea that the electron-rich ancillary ligand destabilizes the $\text{d}\pi$ HOMO, reduces the $^1,^3\text{MLCT}$ energies, and increases the MLCT character in the excited state. This has the consequence of not only red-shifting photoluminescence, but also increasing excited-state spin-orbit coupling and augmenting k_r , leading in many cases to higher Φ_{PL} values. Although this approach did not initially afford great control over k_{nr} , which is another critical determinant of Φ_{PL} , in some of our more recent work on deep-red phosphors we have found that more sterically encumbered L^\wedgeX ligands do result in reduced k_r values. As a result, we have been able to use this strategy to discover two compounds with record-breaking red-phosphorescence quantum yields near 0.8, as well as some compounds with deep-red phosphorescence quantum yields ≥ 0.5 , among the highest ever recorded. In our most recent work on NIR phosphorescence we have found a complementary and effective strategy involving rigid quinoline-derived ancillary ligands, and while the improvements with these designs were modest, the insights they have provided, coupled with our earlier work in the red and deep-red regions, set the stage for continued discovery of state-of-the-art NIR phosphors. Our work until now has focused on unravelling the structure-property relationships and fundamental photophysics of these constructs, but we do believe that these compounds could be enabling platforms for applications in night-vision technology, medical imaging, and biological probes and sensors, which are some of the more applied avenues we are pursuing.

Author contributions

Sungwon Yoon: Visualization, Writing – original draft, Writing – review & editing. **Thomas S. Teets:** Funding acquisition, project administration, Visualization, Writing – original draft, Writing – review & editing.

Conflicts of interest

There are no conflicts to declare.

Acknowledgements

We acknowledge the National Science Foundation (Grant no. CHE-1846831) and Welch Foundation (grant no. E-1887) for funding our group's research on red and near-infrared phosphorescence. We are also grateful to the many previous group members who made important and lasting contributions to the work described in this paper.

Notes and references

- H. Yersin, A. F. Rausch, R. Czerwieniec, T. Hofbeck and T. Fischer, *Coord. Chem. Rev.*, 2011, **255**, 2622–2652.
- H. Yersin, Ed., *Highly efficient OLEDs with phosphorescent materials*, WILEY-VCH, Weinheim, 2008.
- E. Zysman-Colman, Ed., *Iridium(III) in Optoelectronic and Photonics Applications*, John Wiley & Sons, Inc, Chichester, West Sussex, 2017.
- Q. Zhao, F. Li and C. Huang, *Chem. Soc. Rev.*, 2010, **39**, 3007–3030.
- D.-L. Ma, V. P.-Y. Ma, D. S.-H. Chan, K.-H. Leung, H.-Z. He and C.-H. Leung, *Coord. Chem. Rev.*, 2012, **256**, 3087–3113.
- H. Xiang, J. Cheng, X. Ma, X. Zhou and J. J. Chruma, *Chem. Soc. Rev.*, 2013, **42**, 6128–6185.
- X. Wang and O. S. Wolfbeis, *Chem Soc Rev*, 2014, **43**, 3666–3761.
- C. K. Prier, D. A. Rankic and D. W. C. MacMillan, *Chem. Rev.*, 2013, **113**, 5322–5363.
- J.-H. Shon and T. S. Teets, *Comments Inorg. Chem.*, 2020, **40**, 53–85.
- M. A. Baldo, D. F. O'Brien, Y. You, A. Shoustikov, S. Sibley, M. E. Thompson and S. R. Forrest, *Nature*, 1998, **395**, 151–154.
- S. Lamansky, P. Djurovich, D. Murphy, F. Abdel-Razzaq, H.-E. Lee, C. Adachi, P. E. Burrows, S. R. Forrest and M. E. Thompson, *J. Am. Chem. Soc.*, 2001, **123**, 4304–4312.
- M. A. Baldo, S. Lamansky, P. E. Burrows, M. E. Thompson and S. R. Forrest, *Appl. Phys. Lett.*, 1999, **75**, 4–6.
- S. Sprouse, K. A. King, P. J. Spellane and R. J. Watts, *J. Am. Chem. Soc.*, 1984, **106**, 6647–6653.
- M. S. Lowry, W. R. Hudson, R. A. Pascal and S. Bernhard, *J. Am. Chem. Soc.*, 2004, **126**, 14129–14135.
- M. S. Lowry, J. I. Goldsmith, J. D. Slinker, R. Rohl, R. A. Pascal, G. G. Malliaras and S. Bernhard, *Chem. Mater.*, 2005, **17**, 5712–5719.
- S. Lamansky, P. Djurovich, D. Murphy, F. Abdel-Razzaq, R. Kwong, I. Tsyba, M. Bortz, B. Mui, R. Bau and M. E. Thompson, *Inorg. Chem.*, 2001, **40**, 1704–1711.
- T. Sajoto, P. I. Djurovich, A. B. Tamayo, J. Oxgaard, W. A. Goddard and M. E. Thompson, *J. Am. Chem. Soc.*, 2009, **131**, 9813–9822.
- H. Na and T. S. Teets, *J. Am. Chem. Soc.*, 2018, **140**, 6353–6360.
- H. Na, L. M. Cañada, Z. Wen, J. I-Chia Wu and T. S. Teets, *Chem. Sci.*, 2019, **10**, 6254–6260.
- Y. Wu, Z. Wen, J. I.-C. Wu and T. S. Teets, *Chem. – Eur. J.*, 2020, chem.202002775.
- J. Lee, H.-F. Chen, T. Batagoda, C. Coburn, P. I. Djurovich, M. E. Thompson and S. R. Forrest, *Nat. Mater.*, 2016, **15**, 92–98.
- A. K. Pal, S. Krotkus, M. Fontani, C. F. R. Mackenzie, D. B. Cordes, A. M. Z. Slawin, I. D. W. Samuel and E. Zysman-Colman, *Adv. Mater.*, 2018, **30**, 1804231.
- J. D. Bullock, A. Salehi, C. J. Zeman, K. A. Abboud, F. So and K. S. Schanze, *ACS Appl. Mater. Interfaces*, 2017, **9**, 41111–41114.
- A. Tsuboyama, H. Iwawaki, M. Furugori, T. Mukaide, J. Kamatani, S. Igawa, T. Moriyama, S. Miura, T. Takiguchi, S. Okada, M. Hoshino and K. Ueno, *J. Am. Chem. Soc.*, 2003, **125**, 12971–12979.
- C.-H. Fan, P. Sun, T.-H. Su and C.-H. Cheng, *Adv. Mater.*, 2011, **23**, 2981–2985.
- R. Englman and J. Jortner, *Mol. Phys.*, 1970, **18**, 145–164.
- J. S. Wilson, N. Chawdhury, M. R. A. Al-Mandhary, M. Younus, M. S. Khan, P. R. Raithby, A. Köhler and R. H. Friend, *J. Am. Chem. Soc.*, 2001, **123**, 9412–9417.
- M. Penconi, M. Cazzaniga, S. Kesarkar, P. R. Mussini, D. Ceresoli and A. Bossi, *Photochem. Photobiol. Sci.*, 2017, **16**, 1220–1229.
- M. Cocchi, D. Virgili, V. Fattori, J. A. G. Williams and J. Kalinowski, *Appl. Phys. Lett.*, 2007, **90**, 023506.
- K.-H. Kim, J.-L. Liao, S. W. Lee, B. Sim, C.-K. Moon, G.-H. Lee, H. J. Kim, Y. Chi and J.-J. Kim, *Adv. Mater.*, 2016, **28**, 2526–2532.
- B. Carlson, G. D. Phelan, W. Kaminsky, L. Dalton, X. Jiang, S. Liu and A. K.-Y. Jen, *J. Am. Chem. Soc.*, 2002, **124**, 14162–14172.
- A. D. Ryabov, V. S. Soukharev, L. Alexandrova, R. Le Lagadec and M. Pfeffer, *Inorg. Chem.*, 2003, **42**, 6598–6600.
- J.-J. Shen, J.-Y. Shao, Z.-L. Gong and Y.-W. Zhong, *Inorg. Chem.*, 2015, **54**, 10776–10784.
- P.-K. Chow, G. Cheng, G. S. M. Tong, W.-P. To, W.-L. Kwong, K.-H. Low, C.-C. Kwok, C. Ma and C.-M. Che, *Angew. Chem. Int. Ed.*, 2015, **54**, 2084–2089.
- P. Mandapati, J. D. Braun, C. Killeen, R. L. Davis, J. A. G. Williams and D. E. Herbert, *Inorg. Chem.*, 2019, **58**, 14808–14817.
- P. Mandapati, J. D. Braun, I. B. Lozada, J. A. G. Williams and D. E. Herbert, *Inorg. Chem.*, 2020, **59**, 12504–12517.
- V. W.-W. Yam and A. S.-Y. Law, *Coord. Chem. Rev.*, 2020, **414**, 213298.
- L.-K. Li, M.-C. Tang, W.-L. Cheung, S.-L. Lai, M. Ng, C. K.-M. Chan, M.-Y. Chan and V. W.-W. Yam, *Chem. Mater.*, 2019, **31**, 6706–6714.
- W. J. Finkenzeller, M. E. Thompson and H. Yersin, *Chem. Phys. Lett.*, 2007, **444**, 273–279.
- W. J. Finkenzeller, T. Hofbeck, M. E. Thompson and H. Yersin, *Inorg. Chem.*, 2007, **46**, 5076–5083.
- A. P. Marchetti, J. C. Deaton and R. H. Young, *J. Phys. Chem. A*, 2006, **110**, 9828–9838.
- Y. K. Radwan, A. Maity and T. S. Teets, *Inorg. Chem.*, 2015, **54**, 7122–7131.
- J.-H. Shon and T. S. Teets, *Inorg. Chem.*, 2017, **56**, 15295–15303.
- J.-H. Shon, S. Sittel and T. S. Teets, *ACS Catal.*, 2019, **9**, 8646–8658.
- P.-N. Lai, C. H. Brysacz, M. K. Alam, N. A. Ayoub, T. G. Gray, J. Bao and T. S. Teets, *J. Am. Chem. Soc.*, 2018, **140**, 10198–10207.
- P. Lai and T. S. Teets, *Chem. – Eur. J.*, 2019, **25**, 6026–6037.
- E. Kabir, Y. Wu, S. Sittel, B.-L. Nguyen and T. S. Teets, *Inorg. Chem. Front.*, 2020, **7**, 1362–1373.
- A. Kapturkiewicz, J. Nowacki and P. Borowicz, *Electrochimica Acta*, 2005, **50**, 3395–3400.
- J. C. Deaton, R. H. Young, J. R. Lenhard, M. Rajeswaran and S. Huo, *Inorg. Chem.*, 2010, **49**, 9151–9161.
- Y.-J. Su, H.-L. Huang, C.-L. Li, C.-H. Chien, Y.-T. Tao, P.-T. Chou, S. Datta and R.-S. Liu, *Adv. Mater.*, 2003, **15**, 884–888.
- H.-C. Li, P.-T. Chou, Y.-H. Hu, Y.-M. Cheng and R.-S. Liu, *Organometallics*, 2005, **24**, 1329–1335.
- J. M. Fernandez-Hernandez, E. Longhi, R. Cysewski, F. Polo, H.-P. Josel and L. De Cola, *Anal. Chem.*, 2016, **88**, 4174–4178.
- C. You, D. Liu, F. Meng, Y. Wang, J. Yu, S. Wang, S. Su and W. Zhu, *J. Mater. Chem. C*, 2019, **7**, 10961–10971.
- H. U. Kim, H. J. Jang, W. Choi, M. Kim, S. Park, T. Park, J. Y. Lee and K. S. Bejoymohandas, *J. Mater. Chem. C*, 2019, **7**, 4143–4154.
- R. Tao, J. Qiao, G. Zhang, L. Duan, L. Wang and Y. Qiu, *J. Phys. Chem. C*, 2012, **116**, 11658–11664.
- C.-L. Ho, H. Li and W.-Y. Wong, *J. Organomet. Chem.*, 2014, **751**, 261–285.

- 57 Z. Chen, H. Zhang, D. Wen, W. Wu, Q. Zeng, S. Chen and W.-Y. Wong, *Chem. Sci.*, 2020, **11**, 2342–2349.
- 58 P.-N. Lai, S. Yoon and T. S. Teets, *Chem. Commun.*, 2020, **56**, 8754–8757.
- 59 S. Zhang, M. Hosaka, T. Yoshihara, K. Negishi, Y. Iida, S. Tobita and T. Takeuchi, *Cancer Res.*, 2010, **70**, 4490–4498.
- 60 X. Zheng, X. Wang, H. Mao, W. Wu, B. Liu and X. Jiang, *Nat. Commun.*, 2015, **6**, 5834.
- 61 T. Yoshihara, S. Murayama, T. Masuda, T. Kikuchi, K. Yoshida, M. Hosaka and S. Tobita, *J. Photochem. Photobiol. Chem.*, 2015, **299**, 172–182.
- 62 I. S. Kritchenkov, P. S. Chelushkin, V. V. Sokolov, V. V. Pavlovskiy, V. V. Porsev, R. A. Evarestov and S. P. Tunik, *Organometallics*, 2019, **38**, 3740–3751.
- 63 J. Guo, J. Zhou, Guorui Fu, Y. He, W. Li and X. Lü, *Inorg. Chem. Commun.*, 2019, **101**, 69–73.
- 64 S. Kappaun, S. Sax, S. Eder, K. C. Möller, K. Waich, F. Niedermair, R. Saf, K. Mereiter, J. Jacob, K. Müllen, E. J. W. List and C. Slugovc, *Chem. Mater.*, 2007, **19**, 1209–1211.
- 65 H.-R. Park and Y. Ha, *J. Nanosci. Nanotechnol.*, 2012, **12**, 1365–1370.
- 66 G. Zhang, H. Zhang, Y. Gao, R. Tao, L. Xin, J. Yi, F. Li, W. Liu and J. Qiao, *Organometallics*, 2014, **33**, 61–68.
- 67 Z.-T. Yu, Y.-J. Yuan, J.-G. Cai and Z.-G. Zou, *Chem. - Eur. J.*, 2013, **19**, 1303–1310.